

# UV screening clear coats based on encapsulated CeO<sub>2</sub> hybrid latexes

[Miren Aguirre](#),<sup>a</sup> [Maria Paulis](#)<sup>a</sup> and [Jose R. Leiza](#)<sup>\*a</sup>

\* Corresponding authors

<sup>a</sup> Institute for Polymer Materials (POLYMAT) and Kimika Aplikatua saila, University of the Basque Country UPV/EHU, Joxe Mari Korta Zentroa, Tolosa Hiribidea 72, 20018 Donostia-San Sebastián, Spain  
E-mail: [jrleiza@ehu.es](mailto:jrleiza@ehu.es)

## Abstract

CeO<sub>2</sub> nanoparticles have been successfully incorporated into acrylic latex particles with an excellent homogeneous distribution (mostly one inorganic particle per polymer particle) and limited aggregation (inorganic nanoparticles predominantly in the 17–26 nm range, when the original cerium oxide dispersion had a volume average diameter of 8 nm). The hydrophobicity and wettability of the inorganic nanoparticles with the monomer mixture and the process used, semibatch emulsion polymerization on a seed produced by miniemulsion polymerization containing the whole load of the metal oxide, were the key aspects to achieve this morphology for the first time at industrially relevant solids content (40 wt%). Furthermore, the transparency and the substantially enhanced UV-Vis absorbance capacity make those hybrid acrylic/CeO<sub>2</sub> dispersions excellent candidates for a large number of applications including clear coatings and cosmetics.



## Introduction

Incorporation of metal oxidenanoparticles into polymer particles has gained plenty of interest due to the wide range of applications of those hybrid materials in fields like coatings, adhesives, medicine and cosmetics. With the incorporation of inorganic nanoparticles into the polymeric matrix, enhanced mechanical, optical and adhesive properties as well as new functionalities and applications have been discovered.<sup>1-5</sup>

In the field of hybrid outdoor coatings, the purpose of the metal oxidenanoparticles is to protect the substrate, for example, wood, plastic or metals, from weathering agents like sunlight energy, wind and rain. Traditionally, organic UV absorbers have been used to

protect several materials against sunlight. For instance, organic pigments have been successfully incorporated by miniemulsion polymerization in several coatings.<sup>6,7</sup> However, due to environmental concerns and in order to avoid volatile organic compounds (VOC), inorganic nanoparticles have emerged as alternative candidates for UV absorbers. Thus, inorganic nanoparticles such as TiO<sub>2</sub>,<sup>8</sup> ZnO<sup>9,10</sup> or CeO<sub>2</sub> (ref. 11) have been used to enhance the UV absorption capacity of the polymeric material. Their band gap energy is around 3 eV (ref. 12) and they absorb close to 400 nm,<sup>13</sup> which makes them good candidates for UV filtering purposes. Fine CeO<sub>2</sub> possessing a lower refractive index, being quite transparent to visible light, but also having excellent ultraviolet radiation absorption properties, and appearing natural on the skin or on wood without imparting an excessively pale, white look, is an ideal candidate as a broad-spectrum inorganic sunscreen.<sup>14</sup>

Nevertheless, when incorporating metal oxides into a polymeric matrix, it is essential to obtain isolated primary particles (below 40 nm) in order to have transparent films.<sup>13</sup> If the hybrid binder to be produced is for a waterborne coating, which reduces drastically the emissions of VOC compared to a solvent-borne one, miniemulsion polymerization seems to be the most adequate production process.<sup>15-17</sup> However, in order to achieve the encapsulation of the inorganic material within the polymer particles, which would avoid a massive aggregation during film formation, it is necessary to increase its compatibility with the monomer/polymer phase and at the same time reduce the compatibility with the aqueous phase.<sup>18</sup> Following this route, the incorporation of some inorganic fillers has been achieved with a higher or lower degree of success: TiO<sub>2</sub>,<sup>19,20</sup> ZnO,<sup>21</sup> calcium carbonate,<sup>22</sup> magnetite,<sup>23-25</sup> quantum dots,<sup>26,27</sup> montmorillonite,<sup>28-30</sup> silica<sup>31,32</sup> and silver.<sup>33</sup>

Although the properties of cerium oxide nanoparticles are well known and the potential benefits of incorporating CeO<sub>2</sub> nanoparticles as mineral screeners into coating applications are actively pursued, as far as the authors know, the synthesis of hybrid acrylic/CeO<sub>2</sub> latexes with industrially relevant solids content ( $\geq 40$  wt%) that form transparent films and with demonstrated better UV absorption and molecular weight distributions similar to conventional acrylic latexes, has not been shown in the open literature. However, there is a strong interest in both academia and industry to synthesize hybrid inorganic-organic materials using CeO<sub>2</sub> nanoparticles. Qi *et al.*<sup>34</sup> prepared CeO<sub>2</sub> nanoparticle-polymer hybrids by electrostatic complexation giving cluster like structures at solids contents as low as 1 wt%. Bourgeat-Lami *et al.*<sup>35</sup> developed a method to stabilize polymethyl methacrylate (PMMA) and polymethyl methacrylate-*co*-butyl acrylate (PMMA-*co*-BA) particles using CeO<sub>2</sub> nanoparticles as Pickering stabilizers. They found that at least 35 wt% of nanoceria particles was necessary to obtain stable latexes at intermediate solids content (25 wt%) which makes these latexes useless for clear coating applications. Hawkett *et al.*<sup>36</sup> developed a method to encapsulate TiO<sub>2</sub> nanoparticles using amphiphilic macro-RAFT agents that contained acrylic acid groups. The macro-RAFT agents adsorbed on the surface of the nanoparticles, and further the monomer was polymerized by semibatch emulsion polymerization, producing hybrid acrylic/TiO<sub>2</sub> latexes. This strategy was very recently followed by Garnier *et al.*<sup>37</sup> and Zgheib *et al.*<sup>38</sup> Garnier *et al.*<sup>37</sup> have synthesized poly(styrene-*co*-methyl acrylate)/cerium oxide hybrid latexes by surfactant-free emulsion polymerization using cerium oxide nanoparticles dispersed in the aqueous phase and modified with random macro-RAFT agents composed of acrylic acid and *n*-butyl acrylate monomers. A good distribution of the CeO<sub>2</sub> nanoparticles in the polymer particles was obtained and the CeO<sub>2</sub> nanoparticles were located close to the particle-aqueous phase interface. Zgheib *et al.*<sup>38</sup> obtained

composite polyBA/CeO<sub>2</sub> and poly(BA-*co*-MMA)/CeO<sub>2</sub> latexes using similar macro-RAFT agents (based on acrylic acid (AA) and BA monomers in different compositions and of different lengths). Although encapsulation of the CeO<sub>2</sub> nanoparticles was achieved in some examples, the control of the distribution of the CeO<sub>2</sub> nanoparticles was poor and large nanoceria aggregates were observed in the polymer particles. Furthermore, the low conversions achieved during the polymerizations (<70%) and the low solids content used made the latexes inappropriate for applications in coatings. Unfortunately, none of the two references above presented any information about the molecular weight distribution of the latexes (which can be substantially affected by the presence of the macro-RAFT agents) and about the film properties (UV absorption).

As discussed above, the incorporation of CeO<sub>2</sub> nanoparticles into polymeric binders at industrial-like solids content for clear coat applications is challenging and has not been reported. In this work, we present, for the first time, a synthetic route to integrate organically modified CeO<sub>2</sub> nanoparticles into methyl methacrylate/*n*-butyl acrylate/acrylic acid (MMA/BA/AA) copolymer latexes at industrially relevant solids content for UV absorbing coating applications. The approach is based on the formation of a hybrid seed containing all the nanoceria by miniemulsion polymerization and the growth of the seed by semibatch conventional emulsion polymerization. The hybrid latexes (MMA/BA/AA: 49.5/49.5/1 wt%) were synthesized with a solids content of 40 wt%. The microstructure of the polymer was characterized in terms of molecular weight distribution and gel content. The morphology of the resulting hybrid latexes and films was characterized by Transmission Electron Microscopy (TEM). The films casted from these latexes were transparent and showed excellent UV absorption that increased with the amount of cerium oxide nanoparticles in the hybrid latex.

## Experimental part

### Materials

The hydrophobically modified and commercially available CeO<sub>2</sub> dispersion (BYK, Germany) was received in mineral spirits (49 wt%) and it was dried (at 60 °C for two days) before use. Methyl methacrylate (MMA, Quimidroga), butyl acrylate (BA, Quimidroga) and acrylic acid (AA, Fluka) were used as monomers. Potassium persulfate (KPS, Fluka) initiator was used as supplied. Dodecyl diphenyloxide disulfonate (Dowfax 2A1 45%, Dow Chemicals) and *n*-octadecyl acrylate (97%, Aldrich) were used as anionic emulsifier and costabilizer, respectively. Deionized water was used in the miniemulsions and hydroquinone (Fluka) was used for stopping the reaction in the samples withdrawn from the reactor. GPC grade tetrahydrofuran (THF, Scharlab) and technical grade TFH (Scharlab) were used as received for Gel Permeation Chromatography (GPC) analysis and Soxhlet extraction.

### Characterization techniques

CeO<sub>2</sub> nanoparticle, polymer particle and monomer droplet size distributions were measured by Dynamic Light Scattering (DLS) using a Zetasizer Nano Series (Malvern Instruments). For this analysis, a fraction of latex (or miniemulsion) was diluted with deionized water, whereas in the case of the nanoparticle dispersions they were measured

as received. The reported average particle size (droplet size) values represent an average of two repeated measurements.

The stability of the miniemulsions was studied by measuring the backscattered light over time at 60 °C using the Turbiscan Lab Expert equipment. Conversion was measured by gravimetric analysis along the reaction.

The gel fractions of the samples were measured *via* conventional Soxhlet extraction using technical grade tetrahydrofuran (THF) as solvent and calculated as shown elsewhere.<sup>39</sup> Molecular weight distributions were determined by GPC. The samples were dried at room temperature and dissolved in THF. The solutions were filtered (polyamide 0.45 µm) before injection into the GPC, which consisted of a pump (Shimadzu LC-20AD), three columns (Styragel HR2, HR4 and HR6) and a refractive index detector (Waters 2410). Chromatograms were obtained at 35 °C using a THF flow rate of 1 mL min<sup>-1</sup>. The molecular weights obtained were related to polystyrene standards.

The morphology of the latex particles and the films casted from the latexes was analyzed by TEM, TECNAI G2 20 TWIN (FEI), operating at an accelerating voltage of 200 keV in a bright-field image mode. The samples were diluted and stained with 0.5–1 wt% phosphotungstic acid (PTA) and then they were dried using a UV lamp. The films casted at room temperature were trimmed at -40 °C using an ultramicrotome device (Leica EMFC6) equipped with a diamond knife. The ultrathin sections (100 nm) were placed on 300 mesh copper grids and were observed without further staining. Polymer particle and nanoceria particle size distributions were obtained using Image Pro Plus 7.0 software on 500 particles of each kind.

Atomic force microscopy (AFM) was also used to analyze the morphology of the latexes. A multimode AFM (Bruker, Nanoscope V) was used with a TESPW cantilever from Veeco (resonance frequency 286–324 kHz, spring constant 20–80 N m<sup>-1</sup>) operated using the tapping mode. A drop of the sample was casted on a mica surface and applied with a film applicator in order to have a homogeneous surface. The films were dried for an hour at room temperature before being analyzed.

The UV-Vis absorption measurements were carried out using a Shimadzu spectrophotometer (model UV-2550 230 V). The measurements in the 250–600 nm range were done at room temperature on 50 µm films casted in Teflon panels.

## **Polymerization of the hybrid latexes**

Initially, and in order to check the compatibility of the CeO<sub>2</sub> nanoparticles with the acrylic monomer system used as a model binder for coating applications, a fraction of the dried nanoparticles was mixed with the monomer mixture (MMA (49.5 wt%)/BA (49.5 wt%)/AA (1 wt%)). After mixing it magnetically, the mixture was sonified for one minute using a Branson 450 sonifier (operating at 8-output control and 80% duty cycle). The compatibility was assessed both visually and quantitatively by measuring the nanoparticle size once dispersed in the monomer mixture.

As has been pointed out previously, seeded semibatch polymerizations were performed in order to obtain the hybrid latexes at 40% solids content. The seed was produced by miniemulsion polymerization according to the formulation of [Table 1](#). The oil phase was

prepared by dissolving the monomer mixture (MMA/BA/AA: 49.5/49.5/1 wt%), the costabilizer (octadecyl acrylate) and the nanoceria. This mixture was stirred for 15 min at 800 rpm magnetically. The aqueous phase was obtained by dissolving the emulsifier (Dowfax 2A1) in water. Before using a high shear device (sonifier), both phases were magnetically mixed for 15 min. The miniemulsions were then sonified for 5 minutes (operating at 8-output control and 80% duty cycle in an ice bath and under magnetic stirring). The nanoceria amount was changed in the different miniemulsions to obtain final loadings of 0.5 and 1 wt%. The stability of the miniemulsions was studied using the Turbiscan Lab Expert equipment.

Table 1 Formulation used to prepare the miniemulsions at 30 wt% SC

	Component	Wt(%)
Oil phase	MMA	14.85
	BA	14.85
	AA	0.3
	CeO <sub>2</sub> <sup>a</sup>	0–2.5–5
	Octadecyl acrylate <sup>a</sup>	4
Water phase	Dowfax 2A1 <sup>a</sup>	2
	Deionized water	70

**a With respect to the main monomers (MMA/BA/AA).**

The 30 wt% solids content miniemulsions were polymerized batchwise in a 1 L glass jacketed reactor fitted with a reflux condenser, a sampling device, a N<sub>2</sub> inlet and a stirrer rotating at 150 rpm. The temperature was controlled by an automatic control system (Camile TG, CRW Automation Solutions). The miniemulsion was charged in the reactor and after reaching the desired temperature (75 °C) a shot of KPS initiator (0.5 wbm%) was added. The reaction was carried out for half an hour. Once the seed was produced this way, another shot of initiator (KPS, 0.5 wbm%) was added to the reactor and the feeding of a preemulsion (MMA/BA/AA, Dowfax 2A1 1 wbm% and water) of the rest of the monomer amount needed to reach 40% solids content was started. The feeding was carried out for four hours and the reaction mixture was cooked for one more hour at 90 °C. [Table 2](#) displays the different latexes obtained by this semibatch process, with an indication of the nanoceria content in the final formulation. As it can be seen, a blank latex (Run 1) without nanoceria was also synthesized for comparison purposes.

Table 2 Polymerizations carried out using different amounts of CeO<sub>2</sub>

Sample	CeO <sub>2</sub> (%)	Final latex SC (%)	Polymerization method
Run 1	0	40	Semi-batch
Run 2	0.5	40	Semi-batch
Run 3	1	40	Semi-batch

## Results and discussion

The hydrophobically modified CeO<sub>2</sub>nanoparticles were received in a dispersion of a mixture of alkanes at a concentration of approximately 49 wt%. [Fig. 1](#) presents the particle size volume distribution of the received dispersion measured by DLS. The volume average particle size of the nanoceria was 8 nm. As discussed above, this

dispersion was dried and the nanoparticles were dispersed in the monomers (MMA/BA/AA). [Fig. 1](#) shows that the nanoceria particles dispersed in the monomer mixture suffered a small shift to larger sizes. The new dispersion volume average particle diameter was 12 nm. The dispersion obtained was transparent ([Fig. 2](#)), which was a clear indication of the good compatibility of the nanoparticles with the monomer mixture.

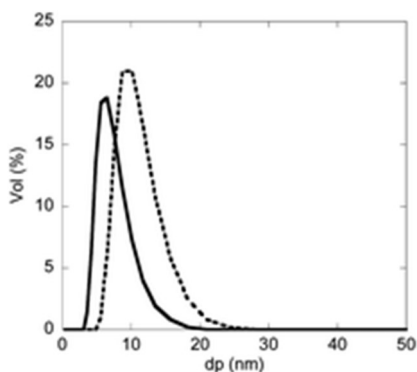


Fig. 1 CeO<sub>2</sub> particle size volume distribution obtained by DLS, in the original dispersion in mineral spirits (continuous line) and in the monomer mixture (dashed line).

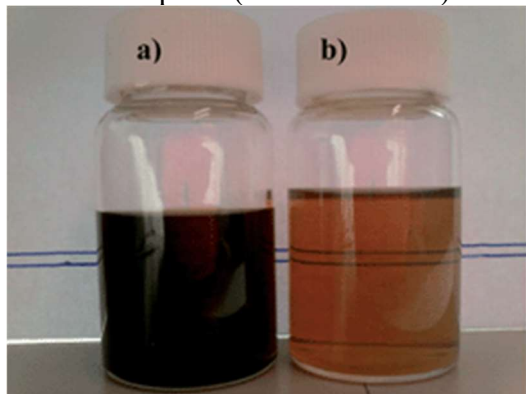


Fig. 2 Dispersion of the CeO<sub>2</sub> nanoparticles in the (a) original dispersion (49 wt%) and (b) monomer mixture (2.5 wt%).

[Fig. 3](#) displays the stability of the miniemulsion prepared with 2.5 wbm% of CeO<sub>2</sub> at 30% solids content at 60 °C. The stability is not complete, but it can be seen that in 30 minutes, the reaction time for this miniemulsion, the degradation of the initial miniemulsion is negligible.

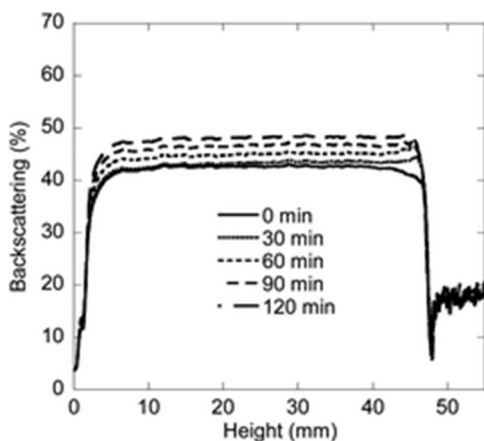


Fig. 3 Stability measurement of the miniemulsion prepared to produce the seed of Run 2 at 60 °C (2.5 wbm% CeO<sub>2</sub>).

Fig. 4 presents the evolution of the instantaneous conversion and particle size during the polymerization reactions. The vertical dashed line represents the time at which the batch miniemulsion polymerization to produce the seed was finished and the preemulsion feeding was started.

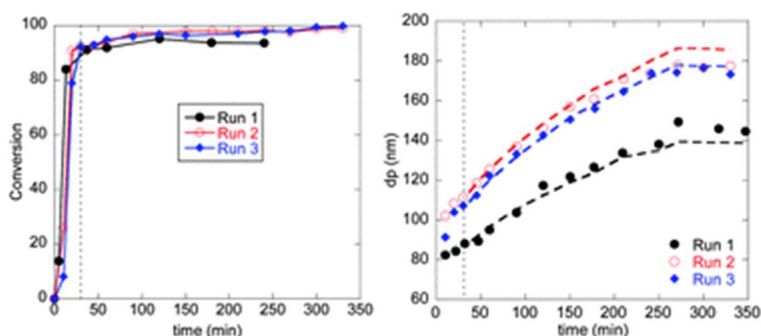


Fig. 4 Instantaneous conversion and particle diameter evolution during the polymerization for Run 1 (0% CeO<sub>2</sub>), Run 2 (0.5% CeO<sub>2</sub>) and Run 3 (1% CeO<sub>2</sub>). The vertical dashed line represents the start of the semibatch feeding and the colored dashed lines represent the theoretical evolution of the particle size in the absence of new nucleations.

Interestingly and contrary to other works where the nanoceria particles are used in emulsion polymerization reactions,<sup>37,38</sup> total conversion was achieved at the end in all the cases and the instantaneous conversions demonstrate that the feeding was done under starved conditions. Regarding the particle size evolution during the reaction, two main conclusions can be drawn. On the one hand, the experimental evolution of the average particle size fits very well with the theoretical evolution calculated considering the growth of the seed particles and excluding secondary nucleations. On the other hand, it can be pointed out that the final particle size of the hybrid latexes was larger than that of the blank latex. In fact, the initial droplet size of the miniemulsion used to prepare the seed (see Table 3) was also larger in the case of the hybrids. This can be explained by the increase of the viscosity of the organic phase in the presence of nanoceria. The higher the viscosity of the organic phase, the larger the droplet size of the miniemulsion for the same amount of energy applied.<sup>17</sup>

Table 3 Summary of the different polymerizations carried out and their final conversion (%), initial droplet size ( $D_d$ , nm), final particle diameter ( $D_p$ , nm), THF insoluble fraction (%) and weight-average molecular weight ( $M_w$ , g mol<sup>-1</sup>)

Sample	CeO <sub>2</sub> (%)	Conversion (%)	$D_d$ (nm)	$D_p$ (nm)	THF ins (%)	$M_w$ (g mol <sup>-1</sup> )
Run 1	0	93	60	145	33	481 000
Run 2	0.5	99	80	165	50	355 000
Run 3	1	100	86	173	52	321 000

The molecular weights of the latexes were not affected by the CeO<sub>2</sub> nanoparticles and they were in the typical range of acrylic binders for coatings (Table 3). This represents an important achievement, as these high molecular weights might be difficult to achieve when macro-RAFT agents are used to stabilize CeO<sub>2</sub> nanoparticles as in ref. 37 and 38. The latexes also presented a significant amount of insoluble polymer. This was not expected because the copolymerizations of BA/MMA in the ratio 50/50 (wt/wt) under similar polymerization conditions did not yield gel or the gel yield was lower than 10–15

wt%.<sup>40</sup> Nevertheless, the presence of 1% of AA has been found to be responsible for the formation of physical gel in latexes,<sup>41,42</sup> which could explain the moderate amounts of gel found in the blank latex. Nevertheless, the incorporation of CeO<sub>2</sub>nanoparticles slightly increased this amount of insoluble polymer and this was attributed to the dispersing agent (not disclosed by the manufacturer) used to stabilize the nanoparticles, which could interact with the growing radicals creating some sort of a crosslinked structure, which is currently being investigated.

**Fig. 5** presents the TEM micrographs of the two hybrid latexes synthesized semi-batchwise with 0.5 and 1 wbm% of CeO<sub>2</sub>nanoparticles (Run 2 (a) and Run 3 (b)) and the distribution of the number of CeO<sub>2</sub>nanoparticles per polymer particle in each case. The micrographs show that the CeO<sub>2</sub>nanoparticles were preferentially incorporated into the polymer particles, as no inorganic particles could be found in the aqueous phase. Furthermore, it is remarkable that every polymer particle contained on average a single CeO<sub>2</sub>nanoparticle. The number of polymer particles with zero, two and three nanoparticles was very small in both cases. The fact that the number of polymer particles without nanoceria is rather small is in very good agreement with the particle size evolution during the reaction, which matched well with the theoretical prediction that assumed secondary nucleation to be negligible and the assumption that all initial droplets contained nanoceria. Regarding the location of the inorganic nanoparticles within the polymeric particles, they are preferentially encapsulated.

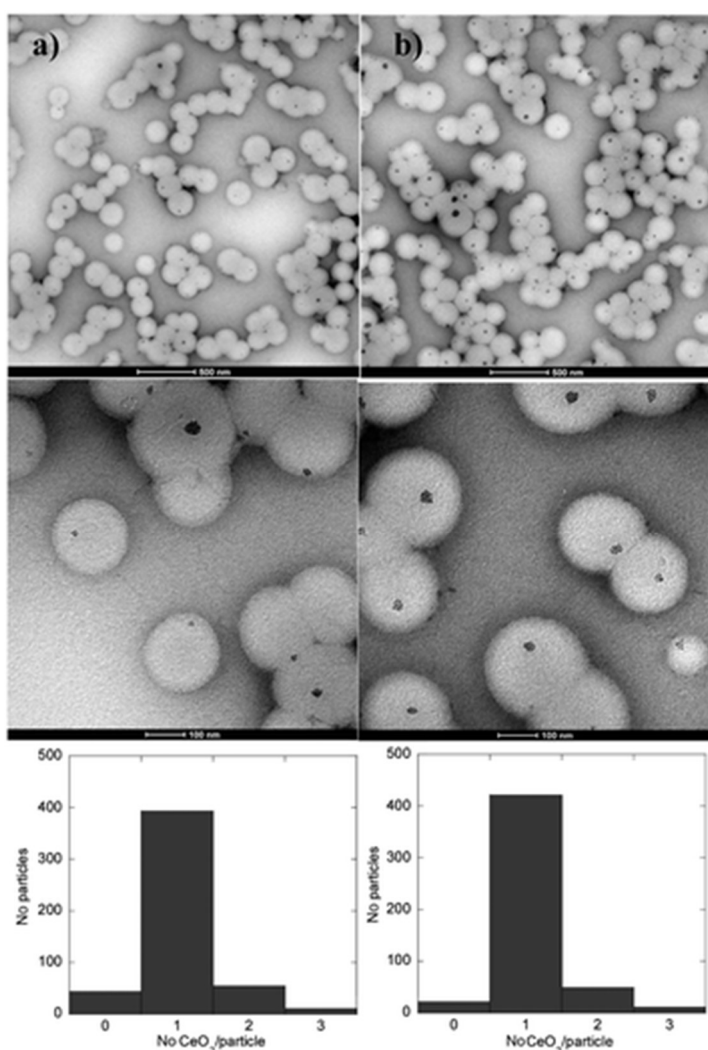




Fig. 5 TEM micrographs and distribution of the number of CeO<sub>2</sub>nanoparticles per polymer particle of poly MMA/BA/AA latexes synthesized with different loadings of CeO<sub>2</sub>nanoparticles: (a) 0.5 wt% and (b) 1 wt%.

[Fig. 6](#) presents the TEM micrograph corresponding to a hybrid latex prepared batchwise by miniemulsion polymerization with 1 wt% of CeO<sub>2</sub> (in the same way as the seed latexes of Runs 1–3 were prepared) for comparison purposes. Interestingly the morphology of the hybrid particles is rather different and the nanoceria particles are predominantly located at the surface of the polymer particles, that is, close to the polymer–aqueous phase interface.

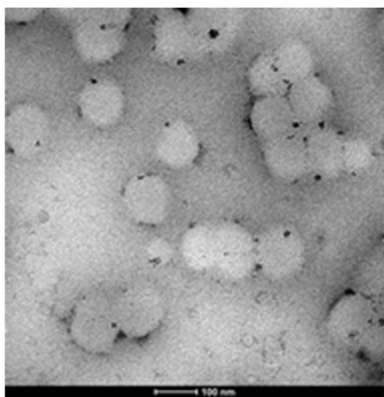


Fig. 6 TEM micrograph of poly MMA/BA/AA latex synthesized with 1 wt% of CeO<sub>2</sub>nanoparticles batchwise.

[Fig. 7](#) presents a comparison of AFM micrographs of the hybrid latex prepared batchwise and Run 3 prepared semibatchwise with the same amount of nanoceria (1 wt%). A droplet of the latex was casted on a mica surface and it was dried for one hour before analysis. The small brighter dots are the CeO<sub>2</sub>nanoparticles, while the darkest regions correspond to wet domains. There is a clear difference in the number of CeO<sub>2</sub>nanoparticles present on the surface of the polymer particles, being much larger for the hybrid latex prepared batchwise. Comparing the two techniques (TEM and AFM), it can be concluded that in the latex synthesized batchwise most of the nanoceria were located at the interface between polymer and water, whereas in the latex synthesized semibatchwise, the nanoceria were preferentially inside the polymer particles. This means that in the miniemulsion process to produce the seed, the nanoceria particles tend to migrate to the particle–aqueous phase interface likely due to the low viscosity of the monomer droplets and the partial hydrophilic character of the modified CeO<sub>2</sub>. However at the end of this stage the viscosity of the particle substantially increased (high conversions were achieved as shown in [Fig. 4](#)) and due to the starved feed of the monomer it remained high. Thus, migration of the nanoparticles during the second stage was constrained and hence a shell of polymer encapsulated them leading to the morphologies shown in [Fig. 5](#).

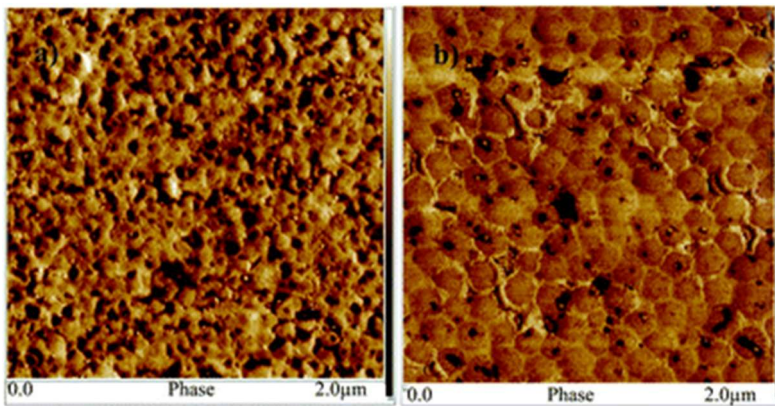


Fig. 7 AFM phase micrographs of hybrid poly (MMA/BA/AA) latexes (1 wt% CeO<sub>2</sub>nanoparticles) prepared (a) batchwise and (b) semibatchwise (Run 3). Samples were casted on a mica surface and the images are 2 μm × 2 μm.

Further proof of the encapsulated morphology of the nanoceria in latexes Run 2 and 3 was obtained by analyzing the TEM at tilted angles. Fig. 8 presents the untilted (b) and tilted images of a polymer particle containing a CeO<sub>2</sub>nanoparticle in latex Run 3. It can be seen that even if the polymer particle is tilted the nanoceria continues appearing in the middle, reinforcing the argument of the encapsulation of the inorganic nanoparticles inside the polymer particles in the semibatch process.

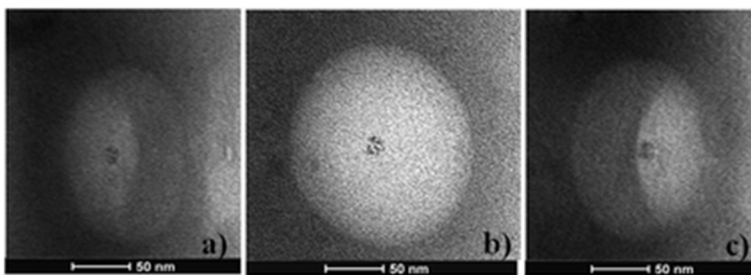


Fig. 8 TEM micrographs of poly MMA/BA/AA latex synthesized with 1 wt% of CeO<sub>2</sub>nanoparticles semibatchwise (Run 3): (a) tilted -55°, (b) untilted and (c) tilted 58°.

Not only the number of nanoceria per polymer particle, but also the size distributions of the nanoceria aggregates and of the polymer particles were measured using the Image Pro Plus 7.0 software. The nanoceria particle size distributions of both hybrid latexes are presented in Fig. 9. In Run 2, nanoceria particles in the 3–48 nm range were present, although most of the particles were centered in the 13–18 nm range. For Run 3, nanoceria aggregate sizes increased up to 73 nm with the main population located at 13–33 nm. The volume average sizes of these distributions together with those of the polymer particle sizes are displayed in Table 4.

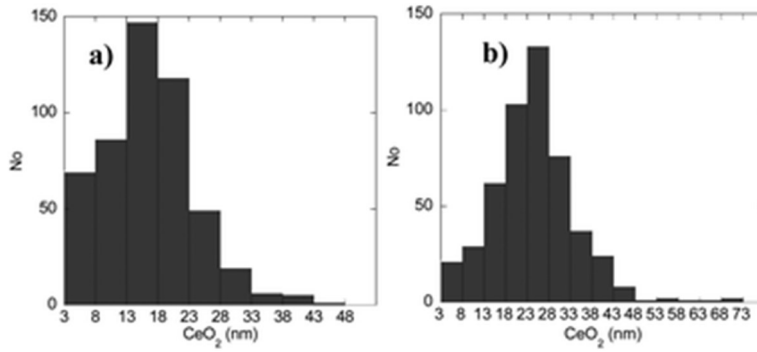


Fig. 9 CeO<sub>2</sub>nanoparticle size

distributions obtained for the latexes with different loadings: (a) 0.5% CeO<sub>2</sub> (Run 2) and (b) 1% CeO<sub>2</sub> (Run 3).

Table 4 Volume average CeO<sub>2</sub>nanoparticle diameter and polymer particle diameter measured by TEM analysis. The theoretical and experimental values of the average nanoceria per polymer particle are also displayed for latexes Run 2 and 3 (40 wt% solids) and batch (30 wt% solids)

	Run 2 (0.5% CeO <sub>2</sub> )	Run 3 (1% CeO <sub>2</sub> )	Batch (1% CeO <sub>2</sub> )
Measured CeO <sub>2</sub> ( $d_{p,CeO_2}$ , nm)	17	26	12
Measured polymer ( $d_p$ , nm)	189	201	114
Measured $N_{p,CeO_2}/N_p^a$	1.2	1.1	1.2
Theoretical $N_{p,CeO_2}/N_p^b$	3.0	7.0	1.4

**a** The number of CeO<sub>2</sub>nanoparticles ( $N_{p,CeO_2}$ ) and the number of polymer particles ( $N_p$ ) were calculated based on the measured volume average particle size calculated

$$N_{p,CeO_2} = \left( m_{CeO_2} / \rho_{CeO_2} \right) / \left[ \frac{4}{3} \pi \left( \frac{d_{p,CeO_2}}{2} \right)^3 \right] \quad \text{and} \quad N_p = \left( M_0 x / \rho_{pol} \right) / \left[ \frac{4}{3} \pi \left( \frac{d_p}{2} \right)^3 \right]$$

from TEM.

where  $m_{CeO_2}$  is the mass of CeO<sub>2</sub>nanoparticles,  $M_0$  is the mass of the monomer in the formulation and  $x$  is the gravimetric conversion. **b** Calculated based on the initial size of the CeO<sub>2</sub>nanoparticle dispersion ( $d_{p,CeO_2} = 12$  nm).

Table 4 shows that the sizes of the nanoceria particles measured in Runs 2 and 3 are larger than those of the original dispersion (12 nm), whereas in the batch process the size was maintained. The seeds used to produce Runs 2 and 3 were also prepared in batch, but the content of the nanoceria was significantly larger than that in experiment batch (2.5 and 5 wt% for Runs 2 and 3, respectively), because the solids content of Runs 2 and 3 was increased to 40 wt% afterwards. The larger concentration of nanoceria particles during seed production likely led to aggregation of particles, which can be clearly observed in the CeO<sub>2</sub>nanoparticle distributions (Fig. 9) and in the average values of Table 4. Therefore, the measured ratio of  $N_{p,CeO_2}/N_p$  is far from the theoretical one in Runs 2 and 3 and close in batch. Note that the volume of an aggregate of 17 nm (Run 2) is the same as the sum of the volumes of three nanoparticles of 12 nm.

An important application of the hybrid acrylic/CeO<sub>2</sub> latexes is as coatings where the transparency and the UV absorption of the films are sought. Transparency of hybrid films is linked to the size of the metal oxides in the films. This was assessed in this work by analyzing the TEM images of cryosectioned films and by measuring the nanoceria particle size distributions. These are shown in Fig. 10 and 11 for the hybrid films with

different CeO<sub>2</sub> loadings (0.5 and 1 wt%). As can be seen in [Fig. 10](#), a very homogeneous distribution of the inorganic nanoparticles was found for both cases.

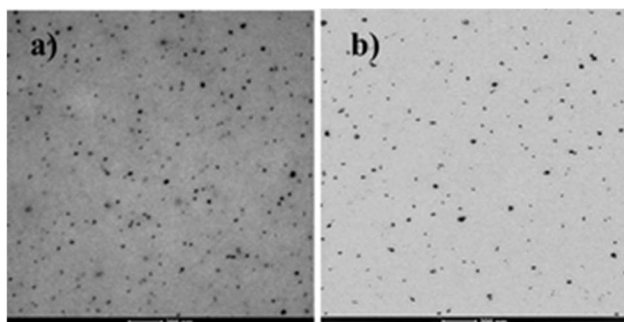


Fig. 10 TEM micrographs of hybrid acrylic/CeO<sub>2</sub> latex films synthesized with different loadings of CeO<sub>2</sub>: (a) 0.5 wt% CeO<sub>2</sub> and (b) 1 wt% CeO<sub>2</sub>.

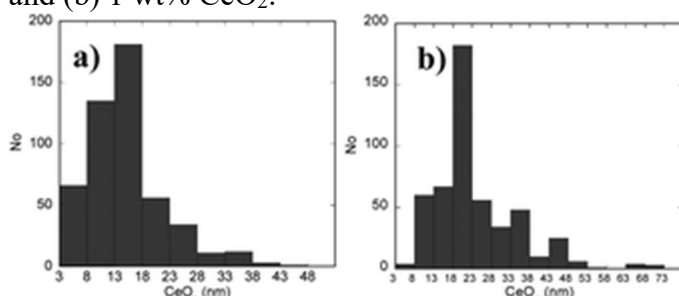


Fig. 11 CeO<sub>2</sub> particle size distribution after film formation for different loadings: (a) Run 2 (0.5% CeO<sub>2</sub>) and (b) Run 3 (1% CeO<sub>2</sub>).

The nanoceria particle size distributions in the film ([Fig. 11](#)) are very similar to those found in the latex ([Fig. 9](#)), which means that little or no aggregation of the nanoceria occurred during the film formation process. This lack of aggregation is certainly favored by the encapsulated morphology of the nanoceria inside the polymer particles.

[Fig. 12](#) demonstrates that all the films were transparent. The homogeneous dispersion of the nanoparticles after the film formation could be the main reason for obtaining transparent films. Note that the color increases with the amount of the nanoparticles from 0.5 wt% to 1 wt%.



Fig. 12 Photographs of films casted for (a) Run 1 (no CeO<sub>2</sub>), (b) Run 2 (0.5 wt% CeO<sub>2</sub>) and (c) Run 3 (1 wt% CeO<sub>2</sub>).

The UV absorption capacity of the hybrid acrylic/CeO<sub>2</sub> films was assessed by measuring the UV absorption of 50  $\mu$ m films cast at room temperature for one day. [Fig. 13](#) presents the UV absorption capacity of the hybrid films (Runs 2 and 3) compared to that of the pure acrylic film (Run 1). The UV absorption of the hybrids was higher in the whole spectrum range (250–600 nm), but most noticeable was the absorption above 300 nm, where the pristine copolymer absorption was almost negligible. Furthermore, the higher is the amount of CeO<sub>2</sub> in the film, the higher is the absorption, although the absorption range is practically the same. Therefore, it has been demonstrated that hybrid

CeO<sub>2</sub>/acrylic binders are a good option for exterior coatings since they are transparent and they absorb more UV-Vis light than conventional acrylic latexes.

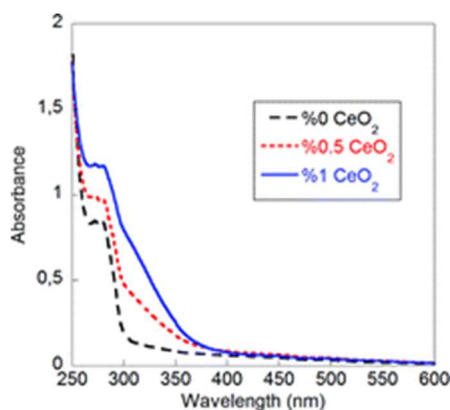


Fig. 13 UV-Vis absorption spectra of hybrid films with different CeO<sub>2</sub> contents: 0% (Run 1), 0.5% (Run 2) and 1% (Run 3).

## Conclusions

Coagulum free acrylic/CeO<sub>2</sub> hybrid latexes were synthesized at 40 wt% solids content with 0.5 and 1 wt% of CeO<sub>2</sub> nanoparticles by seeded semibatch emulsion polymerization. The seed containing all the inorganic particles was produced *in situ* by miniemulsion polymerization. It was found that nanoceria particles were preferentially located at the particle–aqueous phase interface during the miniemulsion polymerization, but in the subsequent seeded semibatch polymerization the nanoparticles were encapsulated as shown by TEM and AFM images. In addition, by increasing the amount of nanoceria in the formulation, the average size of the CeO<sub>2</sub> nanoparticles increased, but on average a single aggregated nanoparticle was found per polymer particle. Aggregation of the original nanoparticles occurred only during the miniemulsion polymerization process, inside each polymer droplet-particle.

Films casted from the hybrid latexes were transparent and showed substantially higher UV absorption than pure copolymer films. UV absorption increased with the amount of CeO<sub>2</sub> in the films. Therefore, these latexes are good candidates for applications in clear coats (*i.e.*, wood coating) and cosmetics due to their excellent UV filtering capability.















## Acknowledgements

Financial support from the European Union (Woodlife project FP7-NMP-2009-SMALL-246434), the Basque Government (GV-IT-303-10) and UPV/EHU (UFI 11/56) is gratefully acknowledged. Miren Aguirre thanks the Basque Government for the scholarship (“*Ikertzaileak prestatzeko eta hobetzeko laguntzak*”). The sGIKER UPV/EHU is acknowledged for the electron microscopy facilities of the Gipuzkoa unit and SGI/IZO-sGIKER UPV/EHU is also gratefully acknowledged.

## References

1. J. Hu, M. Chen and L. Wu, *Polym. Chem.*, 2011, **2**, 760–772 [RSC](#)
2. K. Landfester *Angew. Chem., Int. Ed.*, 2009, **48**, 4488–4507 [CrossRef](#) [CAS](#)

3. M. Paulis and J. R. Leiza , *Advances in Polymer Nanocomposites Technology* , V. MittalNova Science, 2010, [Search PubMed](#) .
4. C. Weiss and K. Landfester , *Hybrid Latex Particles* , A. M. Herk and K. Landfester, Springer, Berlin Heidelberg, 2011, vol. vol. 233, pp. 185–236 [Search PubMed](#) .
5. E. Bourgeat-Lami and M. Lansalot , *Adv. Polym. Sci.*, 2010, **233** , 53 —123 [CrossRef CAS](#) .
6. T. Landuydt and D. Rogez , *Eur. Coat. J.*, 2008, **4** , 34 —38 [Search PubMed](#) .
7. C. Schaller , D. Rogez and A. Braig , *J. Coat. Technol. Res.*, 2012, **9** , 433 —441 [CrossRef CAS](#) .
8. A. Jaroenworoluck , W. Sunsaneeyametha , N. Kosachan and R. Stevens , *Surf. Interface Anal.*, 2006, **38** , 473 —477 [CrossRef CAS](#) .
9. F. Weichelt , R. Emmler , R. Flyunt , E. Beyer , M. R. Buchmeiser and M. Beyer , *Macromol. Mater. Eng.*, 2010, **295** , 130 —136 [CrossRef CAS](#) .
10. H. Zhao and R. K. Y. Li , *Polymer*, 2006, **47** , 3207 —3217 [CrossRef CAS](#) .
11. T. Masui , M. Yamamoto , T. Sakata , H. Mori and G. Adachi , *J. Mater. Chem.*, 2000, **10** , 353 —357 [RSC](#) .
12. C. Fu-Chien and L. Chih-Ming , *J. Phys. D: Appl. Phys.*, 2010, **43** , 075104 [CrossRef](#) . (5pp)
13. J. H. Althues and S. Kaskel , *Chem. Soc. Rev.*, 2007, **36** , 1454 —1465 [RSC](#) .
14. R. Li , S. Yabe , M. Yamashita , S. Momose , S. Yoshida , S. Yin and T. Sato , *Solid State Ionics*, 2002, **151** , 235 —241 [CrossRef CAS](#) .
15. J. Ugelstad , M. S. El-Aasser and J. W. Vanderhoff , *J. Polym. Sci., Polym. Lett. Ed.*, 1973, **11** , 503 —513 [CrossRef CAS](#) .
16. M. Antonietti and K. Landfester , *Prog. Polym. Sci.*, 2002, **27** , 689 —757 [CrossRef CAS](#) .
17. J. M. Asua *Prog. Polym. Sci.*, 2002, **27** , 1283 —1346 [CrossRef CAS](#) .
18. Y. Reyes , M. Paulis and J. R. Leiza , *J. Colloid Interface Sci.*, 2010, **352** , 359 —365 [CrossRef CAS](#) .
19. B. Erdem , E. D. Sudol , V. L. Dimonie and M. S. El-Aasser , *J. Polym. Sci., Part A: Polym. Chem.*, 2000, **38** , 4431 —4440 [CrossRef CAS](#) .
20. R. Faridi-Majidi and N. Sharifi-Sanjani , *J. Appl. Polym. Sci.*, 2007, **105** , 1244 —1250 [CrossRef CAS](#) .
21. H. Lu , B. Fei , J. H. Xin , R. Wang and L. Li , *J. Colloid Interface Sci.*, 2006, **300** , 111 —116 [CrossRef CAS](#) .
22. N. Bechthold , F. Tiarks , M. Willert , K. Landfester and M. Antonietti , *Macromol. Symp.*, 2000, **151** , 549 —555 [CrossRef CAS](#) .
23. J. Ramos and J. Forcada , *Langmuir*, 2011, **27** , 7222 —7230 [CrossRef CAS](#) .
24. L. P. Ramirez and K. Landfester , *Macromol. Chem. Phys.*, 2003, **204** , 22 —31 [CrossRef](#) .
25. L. C. Hong Xu , T. Naihu and G. Hongchen , *J. Am. Chem. Soc.*, 2006, **128** , 15582 —15583 [CrossRef](#) .
26. N. Joumaa , M. Lansalot , A. Théretz , A. Elaissari , A. Sukhanova , M. Artemyev , I. Nabiev and J. H. M. Cohen , *Langmuir*, 2006, **22** , 1810 —1816 [CrossRef CAS](#) .
27. Y. Gao , S. Reischmann , J. Huber , T. Hanke , R. Bratschitsch , A. Leitenstorfer and S. Mecking , *Colloid Polym. Sci.*, 2008, **286** , 1329 —1334 [CrossRef CAS](#) .
28. G. Diaconu , M. Mičušík , A. Bonnefond , M. Paulis and J. R. Leiza , *Macromolecules*, 2009, **42** , 3316 —3325 [CrossRef CAS](#) .

29. G. Diaconu , M. Paulis and J. L. Leiza , *Macromol. React. Eng.*, 2008, **2** , 80 — 89 [CrossRef](#) [CAS](#) .
30. A. Bonnefond , M. Mičušík , M. Paulis , J. R. Leiza , R. Teixeira and S. Bon , *Colloid Polym. Sci.*, 2013, **291** , 167 —180 [CrossRef](#) [CAS](#) .
31. Á. Costoyas , J. Ramos and J. Forcada , *J. Polym. Sci., Part A: Polym. Chem.*, 2009, **47** , 935 —948 [CrossRef](#) .
32. F. Tiarks , K. Landfester and M. Antonietti , *Langmuir*, 2001, **17** , 5775 —5780 [CrossRef](#) [CAS](#) .
33. E. I. López-Martínez , A. Márquez-Lucero , C. A. Hernández-Escobar , S. G. Flores-Gallardo , R. Ibarra-Gómez , M. J. Yacamán and E. A. Zaragoza-Contreras , *J. Polym. Sci., Part B: Polym. Phys.*, 2007, **45** , 511 —518 [CrossRef](#) .
34. L. Qi , J. P. Chapel , J. C. Castaing , J. Fresnais and J. F. Berret , *Soft Matter*, 2008, **4** , 577 —585 [RSC](#) .
35. N. Zgheib , J. L. Putaux , A. Thill , F. D'Agosto , M. Lansalot and E. Bourgeat-Lami , *Langmuir*, 2012, **28** , 6163 —6174 [CrossRef](#) [CAS](#) .
36. D. Nguyen , H. S. Zondanos , J. M. Farrugia , A. K. Serelis , C. H. Such and B. S. Hawkett , *Langmuir*, 2008, **24** , 2140 —2150 [CrossRef](#) [CAS](#) .
37. J. Garnier , J. Warnant , P. Lacroix-Desmazes , P. E. Dufils , J. Vinas , Y. Vanderveken and A. M. van Herk , *Macromol. Rapid Commun.*, 2012, **33** , 1388 —1392 [CrossRef](#) [CAS](#) .
38. N. Zgheib , J. L. Putaux , A. Thil , E. Bourgeat-Lami , F. D'Agosto and M. Lansalot , *Polym. Chem.*, 2013, **4** , 607 —614 [RSC](#) .
39. O. Elizalde , G. Arzamendi , J. R. Leiza and J. M. Asua , *Ind. Eng. Chem. Res.*, 2004, **43** , 7401 —7409 [CrossRef](#) [CAS](#) .
40. I. Gonzalez , J. R. Leiza and J. M. Asua , *Polymer*, 2007, **48** , 2542 —2547 [CrossRef](#) [CAS](#) .
41. J. P. Cohen-Addad , C. Bogonouk and V. Granier , *Macromolecules*, 1994, **27** , 5032 —5036 [CrossRef](#) [CAS](#) .
42. D. I. Lee *Polymer*, 2005, **46** , 1287 —1293 [CrossRef](#) [CAS](#) .